JPE 16-1-27

http://dx.doi.org/10.6113/JPE.2016.16.1.259
ISSN(Print): 1598-2092 / ISSN(Online): 2093-4718

Control Design of the Brushless Doubly-Fed Machines for Stand-Alone VSCF Ship Shaft Generator Systems

Yi Liu*, Wu Ai*, Bing Chen†, and Ke Chen*

†,*School of Mechanical Science and Engineering, Huazhong University of Science and Technology, Wuhan, China

Abstract

This paper presents a stand-alone variable speed constant frequency (VSCF) ship shaft generator system based on a brushless doubly-fed machine (BDFM). In this system, the output voltage amplitude and frequency of the BDFM are kept constant under a variable rotor speed and load by utilizing a well-designed current vector controller to regulate the control winding (CW) current. The control scheme is proposed, and the hardware design for the control system is developed. The proposed generator system is tested on a 325 TEU container vessel, and the test results show the good dynamic performance of the CW current vector controller and the whole control system. A harmonic analysis of the output voltage and a fuel consumption analysis of the generator system are also implemented. Finally, the total efficiency of the generator system is presented under different rotor speeds and load conditions.

Key words: Brushless doubly-fed machine (BDFM), Control scheme, Dynamic performance, Hardware design, Saving-energy performance, Ship shaft generator

I. INTRODUCTION

In recent years, for reducing the energy consumption of ships, the fuel economy performance of ship power generation systems has become a focus of attention for the shipping companies. Ship shaft generator systems, which show excellent saving-energy performance, are becoming the research hotspot. Generally, the main engine of a ship has 10%~15% power redundancies to ensure shipping safety. While the main engine of a ship is driving the propeller, the ship shaft generator system can utilize the redundant power of the main engine for power generation by coupling a generator to the main engine. As a result, a ship shaft generator system can improve the efficiency of the main engine and reduce fuel consumption.

At present, there are three main types of ship shaft generator systems. The first type adopts a synchronous generator and the power electronic converters require the same power rating as the generator [1], [2]. This means that the system cost is very high. The second type is based on a doubly-fed induction machine (DFIM), and the converters only supply slip power to the rotor of the DFIM [3], [4]. The power rating of the converters will be decreased in this system and consequently the cost of the system can be reduced substantially. However, DFIMs possess brushes and slip rings, which increase the maintenance costs for the generator. The third type is based on a brushless doubly-fed machine (BDFM), which is a new type of electrical machine that shows potential in replacing the DFIM [5], [6]. Because BDFMs do not have brushes or slip rings, they are more simple and reliable than DFIGs.

The stator of a BDFM contains two separate windings with different pole numbers (called power winding, PW, and control winding, CW). As a result, BDFMs avoid direct coupling between the two windings. A specially-designed rotor allows for the indirect coupling between the two stator windings.

There are two connection methods between different main engines and a BDFM. For high-speed or medium-speed main engines, the BDFM is directly driven by the main engine, as

Manuscript received Apr. 21, 2015; accepted Jul. 14, 2015
Recommended for publication by Associate Editor Dong-Myung Lee.
†Corresponding Author: chenbing@hust.edu.cn
Tel: +86-027-87541482, Huazhong Univ. of Science and Technology
*School of Mechanical Science and Engineering, Huazhong University of Science and Technology, China

shown in Fig. 1(a). For a low-speed main engine, the BDFM is driven through the connection of a speed-increasing gearbox, as shown in Fig. 1(b).

Many control strategies have been proposed for the variable speed drive applications of BDFMs, such as phase-angle control [7], indirect stator-quantities control [8], and direct torque control [9]. Some control strategies for the BDFMs used as grid-connected wind generators have also been studied, such as the stator-flux-oriented vector control proposed by S. Shao et al. [10]-[12].

Generally, a grid-connected generator system controls the active and reactive power of a generator. Nevertheless, in a stand-alone generator system, the amplitude and frequency of the output voltage of the generator should be stabilized during speed or load changing. Thus, the control scheme of the BDFMs for grid-connected power generators does not directly apply to stand-alone VSCF generator systems. For stand-alone power generation applications, some control systems based on DFIMs have been developed [13]-[16]. However, there are no known studies on the application of a BDFM into stand-alone generation systems.

In this paper, a stand-alone VSCF ship shaft generator system based on a BDFM is presented. The system is tested on a 325 TEU container vessel from the Changjiang National Shipping Group of China. The test results verify the good dynamic performance of the proposed stand-alone VSCF ship shaft generator system. In addtion, harmonic analysis of the output voltage, fuel consumption and total efficiency of the generator system are presented under different rotor speeds and load conditions.

II. Basic Operation Principle of the BDFM

The BDFM can be operated in several modes, including synchronous mode, cascade mode, and induction mode [5]. The synchronous mode, also called the doubly-fed mode, is the optimal mode. Under this mode, the rotor speed can be expressed as follows:

$$\omega_r = \frac{\omega_1 + \omega_2}{p_1 + p_2} \tag{1}$$

where p is the pole pair, and ω is the angular frequency. The subscript 1, 2, and r indicate PW, CW, and rotor, respectively.

When ω_2 is zero, the rotor is rotating at a so-called natural synchronous speed ω_N. Rotor speeds above ω_N are called super-synchronous speeds, and those below ω_N are called sub-synchronous speeds. When the rotor speed varies, to keep ω_1 constant, the value of ω_2 should change with the variation of the rotor speed ω_r, and the expression of ω_2 can be deduced from Equ. (1):

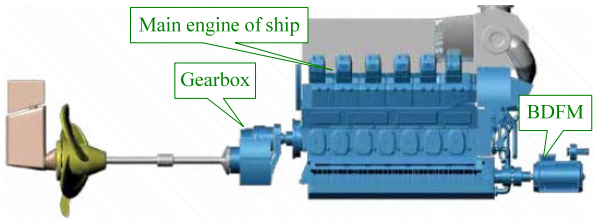

(a) BDFM connection with high-speed or medium-speed main engine.

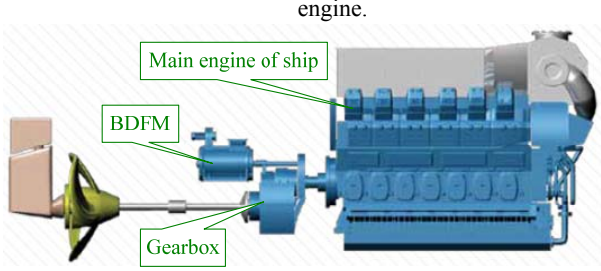

(b) BDFM connection with low-speed main engine.

Fig. 1. Connection methods between different rotation speed engines and BDFM.

$$\omega_2 = \omega_r(p_1 + p_2) - \omega_1 \tag{2}$$

If the copper loss of both the stator and the rotor is ignored, the PW and CW active powers, P_1 and P_2, are in the following relationship [5]:

$$P_1/P_2 = \omega_1/\omega_2 \tag{3}$$

When a BDFM is used in a stand-alone VSCF generator system, PW always outputs power. However, in sub-synchronous operation, the CW will absorb power from the PW, because ω_2 is negative from Equ. (2). This means that the directions of the power flow in the PW and CW are the opposite according to Equ. (3). Similarly, in the super-synchronous operation, the CW will output power to the load.

III. Control Scheme Design

A. Current Vector Control of Control Winding

The dynamic vector model of a BDFM with a wound rotor is expressed as [6], [10]:

$$u_1 = R_1 i_1 + \frac{d\psi_1}{dt} + j\omega_a \psi_1 \tag{4}$$

$$\psi_1 = L_1 i_1 + L_{1r} i_r \tag{5}$$

$$u_2 = R_2 i_2 + \frac{d\psi_2}{dt} + j(\omega_a - (p_1 + p_2)\omega_r)\psi_2 \tag{6}$$

$$\psi_2 = L_2 i_2 + L_{2r} i_r \tag{7}$$

$$u_r = R_r i_r + \frac{d\psi_r}{dt} + j(\omega_a - p_1\omega_r)\psi_r \tag{8}$$

$$\psi_r = L_r i_r + L_{1r} i_1 + L_{2r} i_2 \tag{9}$$

where u, i, and ψ are the voltage, current, and flux; R and L are the resistance and self-inductance; the subscripts 1, 2, and r indicate the PW, CW, and rotor; L_{1r} and L_{2r} are the coupling inductances between the stator windings and the rotor; and ω_a is the angular speed of the dq reference frame.

The proposed CW current vector controller is based on the CW current vector orientation. This means that ω_a in Equs. (4), (6), and (8) should be set as ω_2. The expression $\omega_2 - p_1\omega_r = -(\omega_1 - p_2\omega_r)$ can be derived from Equ. (2). If Equs. (8)-(9) are split into dq components, with the rotor voltage $u_r = 0$, then:

$$0 = R_r i_{rd} + s\psi_{rd} + (\omega_1 - p_2\omega_r)\psi_{rq} \tag{10}$$

$$0 = R_r i_{rq} + s\psi_{rq} - (\omega_1 - p_2\omega_r)\psi_{rd} \tag{11}$$

$$\psi_{rd} = L_r i_{rd} + L_{1r} i_{1d} + L_{2r} i_{2d} \tag{12}$$

$$\psi_{rq} = L_r i_{rq} + L_{1r} i_{1q} + L_{2r} i_{2q} \tag{13}$$

where s is the differential operator d/dt.

Substituting Equs. (12)-(13) into Equs. (10)-(11) yields:

$$i_{rd} = -\frac{[L_r s^2 + R_r s + L_r(\omega_1 - p_2\omega_r)^2](L_{1r} i_{1d} + L_{2r} i_{2d})}{(R_r + L_r s)^2 + L_r^2(\omega_1 - p_2\omega_r)^2} - \frac{R_r(\omega_1 - p_2\omega_r)(L_{1r} i_{1q} + L_{2r} i_{2q})}{(R_r + L_r s)^2 + L_r^2(\omega_1 - p_2\omega_r)^2} \tag{14}$$

$$i_{rq} = \frac{\omega_1 - p_2\omega_r}{R_r + L_r s}\left[1 - \frac{L_r^2 s^2 + L_r R_r s + L_r(\omega_1 - p_2\omega_r)^2}{(R_r + L_r s)^2 + L_r^2(\omega_1 - p_2\omega_r)^2}\right] * (L_{1r} i_{1d} + L_{2r} i_{2d}) - \frac{1}{R_r + L_r s}(L_{1r} i_{1q} + L_{2r} i_{2q}) * \left[s + \frac{L_r R_r(\omega_1 - p_2\omega_r)^2}{(R_r + L_r s)^2 + L_r^2(\omega_1 - p_2\omega_r)^2}\right] \tag{15}$$

The first term in (14) can be written as:

$$-\frac{[s^2 + (R_r / L_r)s + (\omega_1 - p_2\omega_r)^2](L_{1r} i_{1d} + L_{2r} i_{2d})}{L_r[s^2 + 2(R_r / L_r)s + (\omega_1 - p_2\omega_r)^2]}.$$

The zeros and poles of this term are very close. As a result, they can cancel each other out. Then, the first term in Equ. (14) can be simplified as $-(L_{1r} i_{1d} + L_{2r} i_{2d}) / L_r$.

$(R_r + L_r s)^2$ in the denominator of the second term of Equ. (14) occupies a small proportion and can be ignored. Then, the second term in (14) can be simplified as:

$$-\left[R_r(L_{1r} i_{1q} + L_{2r} i_{2q})\right] / \left[L_r^2(\omega_1 - p_2\omega_r)\right].$$

Then, Equ. (14) can be simplified as:

$$i_{rd} = -\frac{L_{1r} i_{1d} + L_{2r} i_{2d}}{L_r} - \frac{R_r(L_{1r} i_{1q} + L_{2r} i_{2q})}{L_r^2(\omega_1 - p_2\omega_r)} \tag{16}$$

Similarly, Equ. (15) can be simplified as:

$$i_{rq} = -(L_{1r} i_{1q} + L_{2r} i_{2q}) / L_r \tag{17}$$

Considering that $\omega_2 - (p_1 + p_2)\omega_r = -\omega_1$, splitting Equs. (6) -(7) into dq components results in:

$$u_{2d} = R_2 i_{2d} + s\psi_{2d} + \omega_1\psi_{2q} \tag{18}$$

$$u_{2q} = R_2 i_{2q} + s\psi_{2q} - \omega_1\psi_{2d} \tag{19}$$

$$\psi_{2d} = L_2 i_{2d} + L_{2r} i_{rd} \tag{20}$$

$$\psi_{2q} = L_2 i_{2q} + L_{2r} i_{rq} \tag{21}$$

Substituting Equs. (16)-(17) to Equs. (18)-(21) yields:

$$i_{2d} = K_d u_{2d} + D_d \tag{22}$$

$$i_{2q} = K_q u_{2q} + D_q \tag{23}$$

where:

$$K_d = K_q = 1/(R_2 + \sigma_2 L_2 \rho)$$

$$D_d = \frac{L_{1r} L_{2r}\rho}{(R_2 + \sigma_2 L_2\rho)L_r} i_{1d} + \frac{L_{1r} L_{2r}[R_r\rho + L_r\omega_1(\omega_1 - p_2\omega_r)]}{(R_2 + \sigma_2 L_2\rho)L_r^2(\omega_1 - p_2\omega_r)} i_{1q} - \frac{\omega_1(\omega_1 - p_2\omega_r)(L_r^2 L_2 + L_{2r}^2 L_r) - L_{2r}^2 R_r\rho}{(R_2 + \sigma_2 L_2\rho)L_r^2(\omega_1 - p_2\omega_r)} i_{2q}$$

$$D_q = -\frac{L_{1r} L_{2r}\left[\omega_1 R_r - L_r(\omega_1 - P_2\omega_r)\rho\right]}{(R_2 + \sigma_2 L_2\rho)L_r{}^2(\omega_1 - P_2\omega_r)} i_{1q} - \frac{\omega_1 L_{1r} L_{2r}}{(R_2 + \sigma_2 L_2\rho)L_r} i_{1d} + \frac{\sigma_2 L_2 L_r\omega_1}{(R_2 + \sigma_2 L_2\rho)L_1} i_{2d}$$

where $\sigma_2 = 1 - L_{2r}^2 / (L_2 L_r)$ is the leakage constant of the CW. K_d and K_q represent the direct relation between i_2 and u_2; D_d and D_q represent the cross-coupling between the PW and the CW, and can be regarded as a low-frequency disturbance changing with the rotor's angular speed ω_r. Fig. 2 shows the control loop of the CW current vector.

B. Overall Control Scheme

The overall control scheme, as shown in Fig. 3, consists mainly of the PW voltage amplitude control, the CW current vector control, the CW current reference frequency calculating, and the actual PW voltage amplitude calculation.

In the PW voltage amplitude control, a PI regulator is employed to regulate the CW current amplitude to keep the PW voltage amplitude constant under variable rotor speed and load conditions. The limiter block in the PW voltage amplitude control ensures that the CW current command will not exceed its rated value. In the CW current vector control, the reference value of the CW current q component i_{2q}^* is set to zero. This means that the reference value of the CW current d component i_{2d}^* is equal to the CW current amplitude reference. The CW current vector angle θ_2^* is obtained via an integration of the reference value of the CW current angular frequency, which is obtained by the CW current reference frequency calculation. Finally, the CW

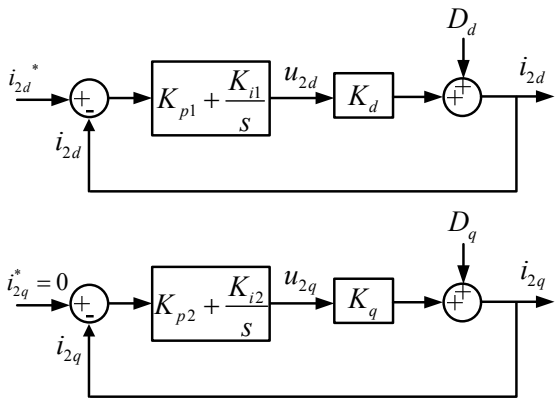

Fig. 2. Control loop of the CW current vector.

current vector controller can generate the excitation current with the corresponding frequency and amplitude in the CW. The actual PW voltage amplitude is gained through a transformation from the three-phase static coordinates to the two-phase static coordinates. The ripple on the PW voltage amplitude U_1 is eliminated by a low-pass filter.

IV. Hardware Design

A. BDFM Design

A 60 kw BDFM with a wound rotor is specially designed for the stand-alone VSCF ship shaft generator system. The design of the rotor winding (RW) utilizes the principles of tooth harmonics and sinusoidal winding [17]. The RW, constituted by double-layer unequal-turn coils, makes the magnetomotive force space vector in one set of three-phase symmetric windings mainly contain two fundamental sinusoidal magnetic fields with different pole pairs. Compared with a nested-loop cage rotor of the same size, the rotor harmonic and refereed rotor leakage reactance is reduced significantly. In addition, this BDFM is optimized for a speed range of 375~700 r/min, which matches the speed range of the main engine in a 325 TEU container vessel. The pole-pair numbers of the PW and CW in the BDFM are 4 and 2, respectively. In addition, the natural synchronous speed is 500 r/min at a PW frequency of 50 Hz. The detailed parameters of the BDFM are listed in TABLE I.

TABLE I
60 kw BDFM Specification

Parameter	Value	Parameter	Value
Frame size	Y315	Stator OD	520 mm
PW pole pairs	4	Stator ID	390 mm
CW pole pairs	2	Rotor OD	388.4 mm
Natural synchronous speed	500 r/min	Stator teeth width	6.0 mm
Speed range	375~700 r/min	Rotor teeth width	8.4 mm
PW rated voltage	400 V	Shaft diameter	100 mm
PW rated current	92 A	Stack length	455 mm
PW freq.	50 Hz	Stator slots	72
CW voltage range	0~320 V	Rotor slots	54
CW current range	0~150 A	L_1	0.2238 H
CW freq. range	-12.5~20 Hz	L_2	0.2457H
R_1	1.43 Ω	L_r	0.0216 H
R_2	0.86 Ω	L_{1r}	0.0637 H
R_r	0.112 Ω	L_{2r}	0.1228 H

B. Control Circuit Design

The structure of the control circuit is shown in Fig. 4. The main engine of the vessel directly drives the rotor of the BDFM. The CW side converter (CSC) supplies the CW with a frequency-variable exciting current. The active front end (AFE), which is from ARADEX Co., Germany, has the major functions of (a) stabilizing the voltage of the DC bus at the setpoint, (b) absorbing the PW power to supply the CW at sub-synchronous speeds, (c) feedbacking the CW power to the PW side at super-synchronous speeds, and (d) maintaining the unity power factor of the AFE AC side. Eight film capacitors are connected in parallel to the DC bus, and each capacitor has a capacitance of 4000uF and a rated DC voltage of 800V. Since the DC bus capacitors are uncharged before the stand-alone BDFM system startup, the CSC cannot run or provide the CW with exciting current. Thus, an initial charging circuit should be added to the system to precharge the DC bus capacitors. The current-limiting resistors in the initial charging circuit ensure that the charging current will not be too large. In addition, a DC Crowbar device is installed into the system to prevent excessively high DC bus voltages from damaging the power devices or capacitors when a fault occurs.

The voltages of the PW and the DC bus are measured by LEM LV 100 sensors, and the currents of the CW are measured via LEM LT 208-S7/SP1 sensors. The position of the rotor is measured by an incremental encoder (RHI90 from P+F Co.), with a resolution of 1024 cycles/r. The controller board is designed based on an ARM (Freescale MK60FN1M0VLQ12) and a FPGA (Altera Cyclone IV). On the controller board, a synchronous sampling ADC chip (AD7606) is used to sample the voltage and current signals. The controller board outputs PWM signals to the CSC to regulate the amplitude and frequency of the CW current. The AFE is controlled by the controller board through CAN bus communications. A touch screen serves as the human machine interface (HMI) for inputting commands and displaying the system status information.

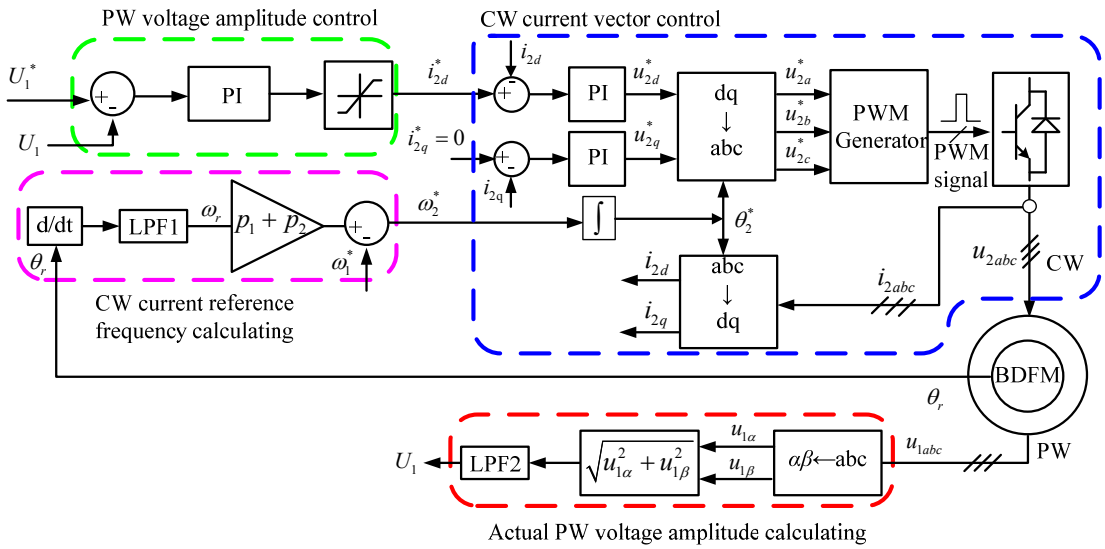

Fig. 3. Block diagram of the overall control scheme.

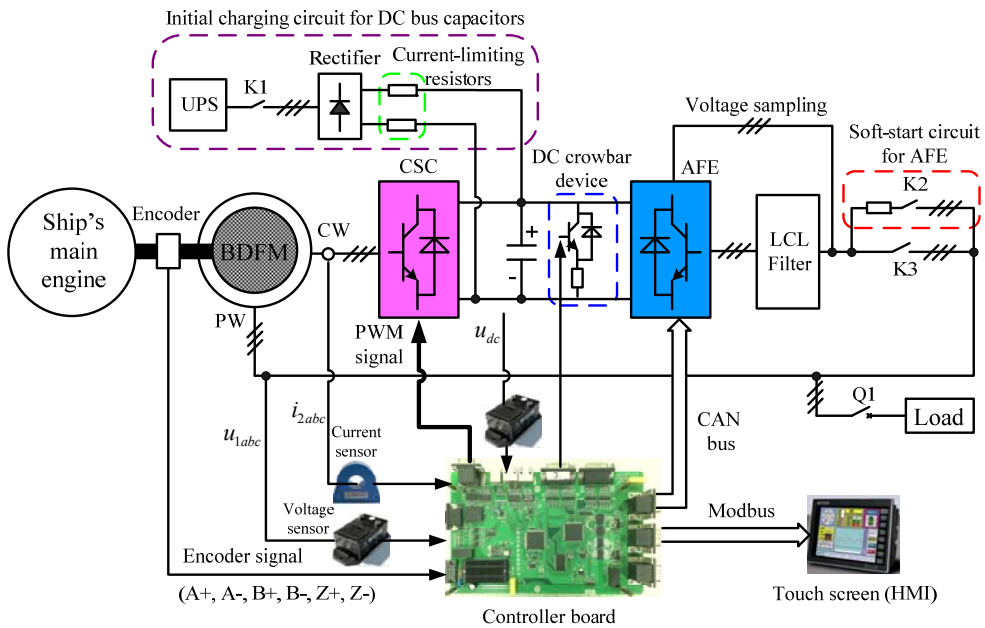

Fig. 4. Block diagram of the control circuit.

V. Operation Results and Analysis

A. Practical Stand-Alone VSCF Ship Shaft Generator System Based on a BDFM

A practical stand-alone VSCF ship shaft generator system based on a BDFM has been built in a 325 TEU container vessel from the Changjiang National Shipping Group of China. The loading capacity and normal electric load of the vessel are 6200 tons and 30 kw, respectively. The power and speed range of the vessel's main engine are 518 kw and 375~700 r/min, respectively. The BDFM is directly coupled to the shaft of the main engine, as shown in Fig. 5. The DC bus voltage of the converter is kept at 800 V. The reference of the output line voltage of the BDFM is 400Veff/50Hz. The cycle time of the control program is 250us, and all of the parameters are tuned using the Ziegler-Nichols Method, which does not require precise knowledge of the BDFM plant model.

B. Simulation and Experiments of the CW Current Vector Controller

Both simulations and experiments have been carried out to test the CW current vector controller's response to step changes in the reference value of i_{2d} at sub-synchronous and super-synchronous speeds.

Test 1: The rotor speed is 400 r/min. At 50 ms, the

reference value of i_{2d} changes from 0 to 30 A, while that of i_{2q} is still 0 A. The given value of ω_2 is -62.8 rad/s according to Equ. (2). Fig. 6(a) shows the results from the simulation and experiment. The overshoot of i_{2d} is 8.36%, with a rising time of 16 ms and a settling time of 50 ms. The current i_{2q} fluctuates with a peak of about 7 A, and it will be stable with the stabilization of i_{2d}.

Test 2: The rotor speed is 600 r/min. The references of i_{2d} and i_{2q} are the same as those in Test 1. The given value of ω_2 is 62.8 rad/s. The experimental result and simulation predictions are shown in Fig. 6(b). The overshoot of i_{2d} is 7.08%, with a rising time of 12 ms and a settling time of 70 ms.

In these two tests, the high consistency between the simulations and the experimental results indicates that the CW current vector controller proposed in this paper is effective. However, the dynamic performance is slightly different in the two tests. This is due to the fact that the two low-frequency disturbances D_d and D_q are related to the rotor's angular speed ω_r. As a result, the dynamic performance of the CW current vector controller varies with the rotor speed. The experimental results of i_{2d} and i_{2q} show high-frequency ripples, which are due to the high-frequency switching of the IGBTs.

C. Dynamic Performance of the Control System

The dynamic performance of the proposed generator system is verified by four different experiments, and the results are shown in Fig. 7-Fig. 10.

In Fig. 7, a step change of the load from 60 kw (full load) to 0 is applied, with the rotor speed of the generator at 600 r/min. When the load suddenly drops, the CW current amplitude decreases rapidly from 79.2 to 28.3 A in one period. A transient increase occurs in the amplitude of the output voltage whose peak value is not more than 8.8% of the rated voltage, which is acceptable to the ship shaft generator system.

Fig. 8 shows the dynamic performance under a load step change from 0 to 42 kw, with the rotor speed of the generator at 400 r/min. When the sudden loading occurs, the amplitude of the output voltage decreases to about 91% of the rated value, and the CW current amplitude increases from 28.2 to 115 A within about 300 ms. After 300 ms, the amplitude of the output voltage recovers.

Fig. 9 and Fig. 10 show the dynamic performance during a rotor speed change. In the two experiments, the generator is connected with a 42 kw load. During the rotor speed change, the output voltage amplitude and frequency are almost constant. The analysis shows that the errors of the output

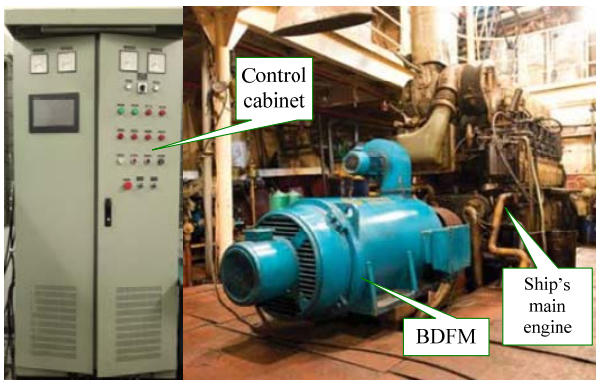

Fig. 5. Photograph of practical stand-alone VSCF ship shaft generator system based on BDFM in a container vessel.

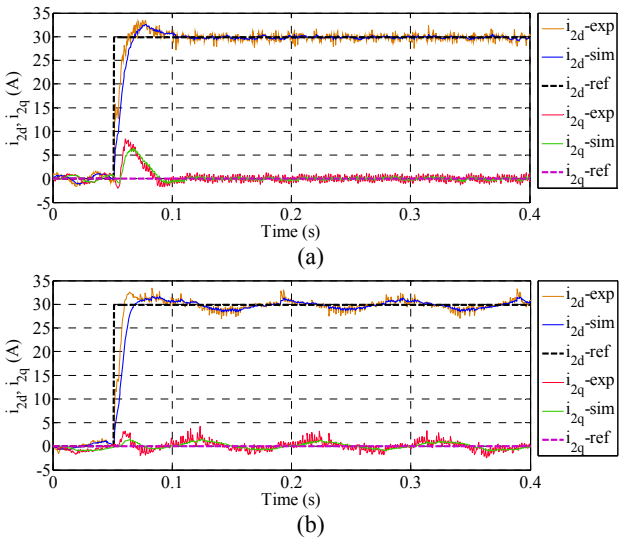

Fig. 6. Simulated and experimental results of CW current vector controller. (a) Results at rotor speed of 400 r/min. (b) Results at rotor speed of 600 r/min.

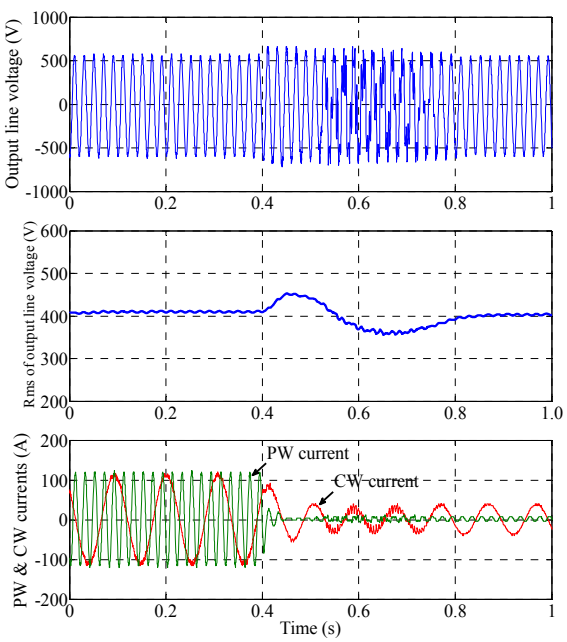

Fig. 7. Dynamic performance for a load step change from 60 kw to 0 (the rotor speed is kept constant at 600 r/min).

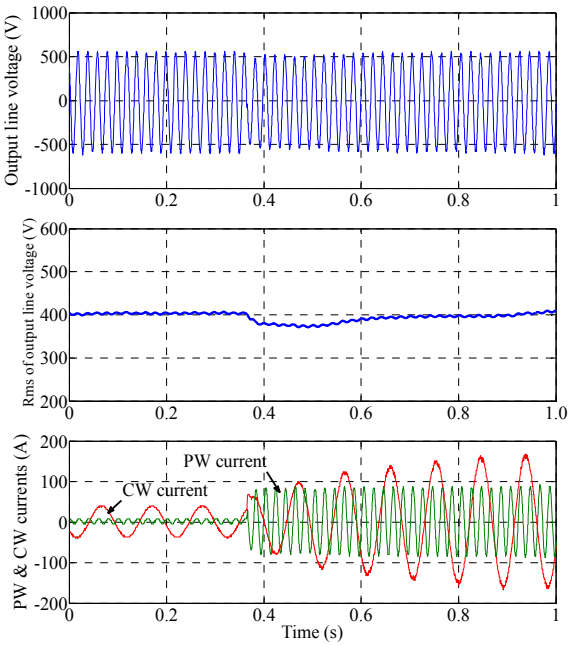

Fig. 8. Dynamic performance for a load step change from 0 to 42 kw (the rotor speed is kept constant at 400 r/min).

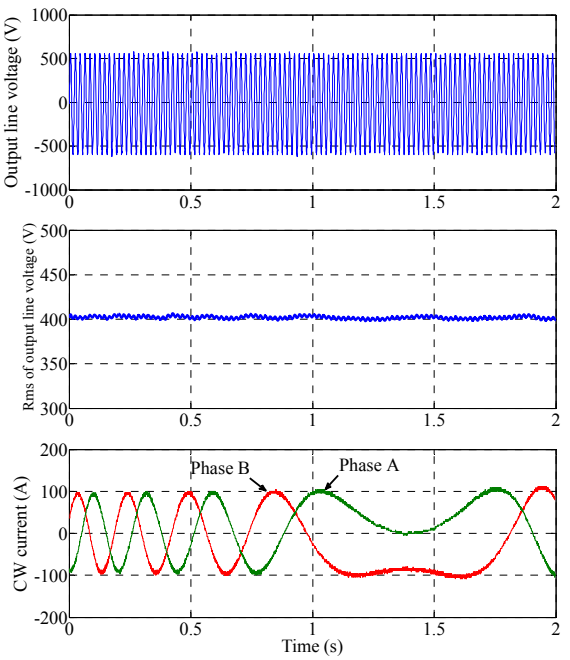

Fig. 9. Dynamic performance for a rotor speed change from super-synchronous to sub-synchronous speed (the load is kept constant at 42 kw).

voltage amplitude and frequency are less than ±1% of the rated values. In addition, as can be seen from Fig. 9 and Fig. 10, the phase sequence of the CW current is changed when the rotor speed is through the natural synchronous speed.

D. Harmonic Analysis of the Output Voltage

In this section, the harmonic content and THD of the output voltage are investigated in the prototype BDFM both with and without a load. For the sake of brevity, the results

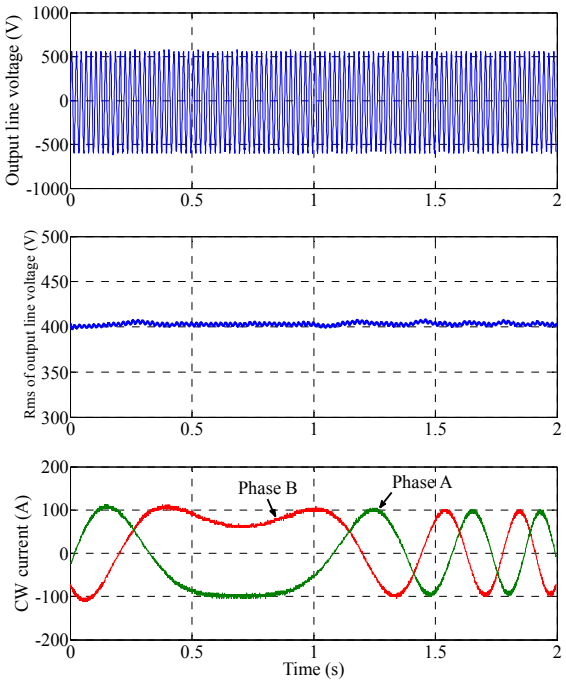

Fig. 10. Dynamic performance for a rotor speed change from sub-synchronous to super-synchronous speed (the load is kept constant at 42 kw).

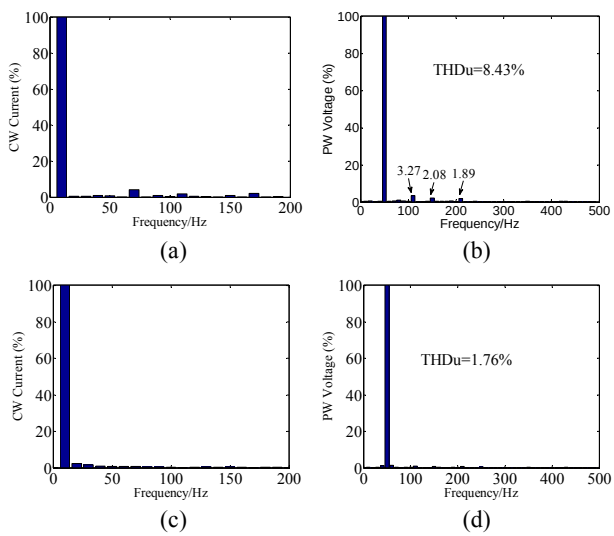

Fig. 11. FFT analysis of PW voltage and CW current under steady-state operation at 600 r/min: (a) FFT analysis result of CW current under no-load condition, (b) FFT analysis result of PW voltage under no-load condition, (c) FFT analysis result of CW current under 60 kw load (full load), and (d) FFT analysis result of PW voltage under 60 kw load (full load).

are given in Fig. 11 for 600r/min rotor speed only. As can be seen from Fig. 11(a), the CW current fundamental frequency is 10 Hz and the CW current contains abundant harmonic components, especially those at 70, 110 and 170 Hz, under the no-load condition. Owing to the cross-coupling effect between the PW and the CW, the CW harmonic components will induce harmonics in the PW whose frequency can be

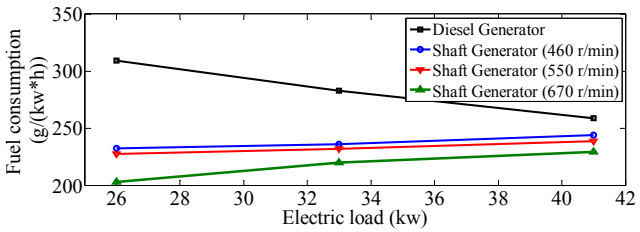

Fig. 12. Fuel consumption of diesel generator and shaft generator.

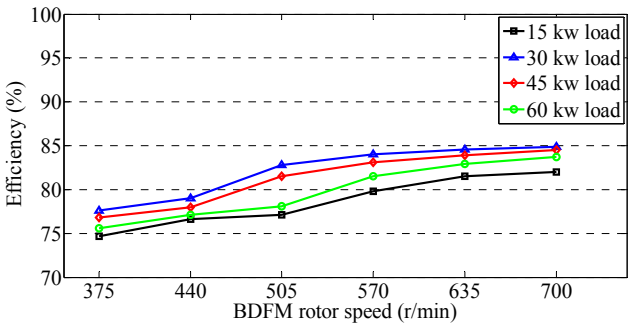

Fig. 13. Total efficiency of the generation system.

decided from (1). This equation indicates that the most significant harmonics in the PW are at 110, 150, and 210 Hz. In fact, as shown in Fig. 11(b), the notable harmonic components of the PW voltage under no load are at 110, 150 and 210 Hz, whose amplitudes are 3.27%, 2.08% and 1.89% of the fundamental component, respectively. Fig. 11(c)–(d) show the harmonic analysis results of the CW current and the PW voltage under a 10 kw load (full load). Clearly, the harmonic contents in the CW and the PW are reduced after loading. The total harmonic distortion rates of the PW voltage under the two conditions are calculated as 8.43% under no load and 1.76% under a full load. Hence, a better quality for the PW voltage can be achieved when the generator is connected with loads.

E. Fuel Consumption Analysis

The average fuel consumption of the shaft generator system based on a BDFM has been measured under different electric loads and rotor speeds over the course of a week. In addition, there is a pre-existing diesel generator, whose rated power is 75 kw, in the 325 TEU container vessel. In order to analyze the economic performance of the shaft generator, its fuel consumption is compared with that of the diesel generator, as shown in Fig. 12. The comparison results demonstrate that the proposed shaft generator system can reduce fuel consumption remarkably. In addition, the higher the rotor speed is, the better the saving-energy performance of the shaft generator system becomes.

F. Total Efficiency of the Generation System

The total efficiency of the generation system has been calculated under different rotor speed and load conditions by measuring the input power from the rotor shaft and the output power to the loads. As shown in Fig. 13, the total efficiency of the generation system based on the BDFM is in the range of 75%~85%, which is slightly lower than the efficiency of a conventional DFIM generation system with the same capacity (typically 80%~90%). However, the BDFM is just an experimental prototype and the design can be further optimized to increase efficiency in the future. It is noteworthy that the efficiency at super-synchronous speeds is higher than that at sub-synchronous speeds under the same load. Therefore, in a stand-alone generation system, the BDFM should operate at super-synchronous speeds as much as possible.

VI. CONCLUSION

A stand-alone VSCF ship shaft generator system based on a BDFM and its control scheme are presented in this paper. The control target of this stand-alone VSCF generator system is that when the rotor speed and load of the generator are changed, the amplitude and frequency of the output voltage are kept constant. The proposed generator system has been tested on a 325 TEU container vessel, and the test results show the excellent dynamic performance, the satisfactory quality of the output voltage, and the good saving-energy performance. The operating time of the diesel generator in the vessel is reduced as a result of the stand-alone operation of the VSCF shaft generator. Hence, the maintenance cost of the vessel power station can be decreased significantly. The present research has demonstrated the great commercial application prospects for the BDFM ship shaft generator system.

Work is presently underway to investigate the grid-connected operation of a BDFM shaft generator system with diesel generator sets.

ACKNOWLEDGMENT

This work was supported by National Natural Science Foundation of China under Grant 51475184 and Grant 51105154. Besides, the authors wish to thank China Changjiang National Shipping Group Motor Factory for their support.

REFERENCES

[1] S. Li, P. X. Yang, L.F. Liu, L. Chen, L. X. Bi, and G. Cui, "Research on grid-connected operation of novel variable speed constant frequency (VSCF) shaft generator system on modern ship," in *Proc. 15th International Conf. Electrical Machines and Systems(ICEMS)*, pp. 1-5, Oct. 2012.

[2] B. H. Gully, M. E. Webber, and C.C. Seepersad, "Shaft motor-generator design assessment for increased operational efficiency in container ships," in *Proc. ASME*

5th Int. Conf. Energy Sustainability, pp. 1813-1819, Aug. 2011.
[3] X. Y. Xu, Y. Z. Ye, and C. Chen, "On control of power supply process of marine shaft generator," in *Proc. IEEE Int. Conf. Systems, Man and Cybernetics*, pp. 4776-4779, Oct. 2009.
[4] L. Peng, Y. D. Li, J. Y. Chai, and G. F. Yuan, "Vector control of a doubly fed induction generator for stand-alone ship shaft generator systems," in *Proc. Int. Conf. Electrical Machines and Systems*, pp. 1033-1036, Oct. 2007.
[5] R. A. McMahon, P. C. Roberts, X. Wang, and P. J. Tavner, "Performance of BDFM as generator and motor," *IEE Proc.-Elect. Power Appl.*, Vol. 153, No. 2, pp. 289–299, Mar. 2006.
[6] F. Xiong, "Research on modeling analysis and electromagnetic design of wound-rotor brushless doubly-fed machine," *Ph.D. Dissertation, Huazhong Univ. of Sci. & Tech., China*, 2010.
[7] S. Shao, E. Abdi, and R. McMahon, "Low-cost variable speed drive based on a brushless doubly-fedmotor and a fractional unidirectional converter," *IEEE Trans. Ind. Electron.*, Vol. 59, No. 1, pp. 317-325, Jan. 2012.
[8] A. Zhang, X. Wang, W. Jia, and Y. Ma, "Indirect stator-quantities control for the brushless doubly fed induction machine," *IEEE Trans. Power Electron.*, Vol. 29, No. 3, pp. 1392-1401, Mar. 2014.
[9] I. Sarasola, J. Poza, M. A. Rodriguez, and G. Abad, "Direct torque control design and experimental evaluation for the brushless doubly fed machine," *Energy Conversion and Management*, Vol. 52, No. 2, pp. 1226-1234, Feb. 2011.
[10] S. Shao, E. Abdi, F. Barati, and R. McMahon, "Stator-flux-oriented vector control for brushless doubly-fed induction generator," *IEEE Trans. Ind. Electron.*, Vol. 56, No. 10, pp. 4220-4228, Oct. 2009.
[11] T. Logan, J. Warrington, S. Shao, and R. McMahon, "Practical deployment of the Brushless Doubly-Fed Machine in a medium scale wind turbine," in *Proc. Int. Conf. PEDS,* pp. 470-475, Nov. 2009.
[12] S. Shao, E. Abdi, and R. McMahon, "Vector control of the brushless doubly-fed machine for wind power generation," in *Proc. Int. Conf. Sustainable Energy Technol.*, pp. 322-327, Nov. 2008.
[13] V.-T. Phan, H.-H. Lee, and T.-W. Chun, "An improved control strategy using a PI-resonant controller for an unbalanced stand-alone doubly-fed induction generator," *Journal of Power Electronics*, Vol. 10, No. 2, pp. 194-202, Mar. 2010.
[14] T. Daido, Y. Miura, T. Ise, and Y. Sato, "Characteristics on stand-alone operation of a doubly-fed induction generator applied to adjustable speed gas engine cogeneration system," *Journal of Power Electronics*, Vol. 13, No. 5, pp. 841-853, Sep. 2013.
[15] K. Vijayakumar, N. Kumaresan, and N. A. Gounden, "Operation and closed-loop control of wind-driven stand-alone doubly fed induction generators using a single inverter-battery system," *IET Electr. Power Appl.*, Vol. 6, No. 3, pp. 162-171, Mar. 2012.
[16] K. Vijayakumar, N. Kumaresan, and N. A. Gounden, "Operation of inverter-assisted wind-driven slip-ring induction generator for stand-alone power supplies," *IET Electr. Power Appl.*, Vol. 7, No. 4, pp. 256-269, Apr. 2013.
[17] F. Xiong and X. Wang, "Design of a low-harmonic-content wound rotor for the brushless doubly fed generator," *IEEE Trans. Energy Convers.*, Vol. 29, No. 1, pp. 158-168, Mar. 2014.

Yi Liu was born in Wuhan, China, in 1982. He received his B.S. and M.S. degrees in Automation and Control Engineering from the Wuhan University of Science and Technology, Wuhan, China, in 2004 and 2007, respectively. From 2007 to 2011, he was with the Wuhan University of Science and Technology as a Lecturer. He is presently working towards his Ph.D. degree in the School of Mechanical Science and Engineering, Huazhong University of Science and Technology, Wuhan, China. His current research interests include AC electrical machine control and inverter systems.

Wu Ai received his B.S. and M.S. degrees in Electrical Engineering from the Huazhong University of Science and Technology, Wuhan, China, in 1979 and 1989, respectively; and his Ph.D. degree in Electronics and Information Engineering from the Hong Kong Polytechnic University, Kowloon, Hong Kong, in 2001. He became an Associate Professor in May 2001, and a Professor in December 2004, at the Center for Numerical Control Engineering, Huazhong University of Science and Technology. His current research interests include power electronics, electrical drives, intelligent control and nonlinear optimum control.

Bing Chen received his B.S. degree in Electrical Engineering from Beijing Jiaotong University, Beijing, China, in 1998. He received his M.S. and Ph.D. degrees in Mechanical Engineering from Huazhong University of Science and Technology, Wuhan, China, in 2002 and 2006, respectively. He is presently an Associate Professor with the School of Mechanical Science and Engineering, Huazhong University of Science and Technology. His current research interests include the modeling and control of electrical machines, motion control and manufacturing automation.

Ke Chen received his B.S. degree from the Central South University, Changsha, China, in 2010. He is presently working towards his Ph.D. degree in the School of Mechanical Science and Engineering, Huazhong University of Science and Technology, Wuhan, China. His current research interests include electrical drives and machine control.